This is a repository copy of *On the importance of antimony for temporal evolution of emission from self-assembled (InGa)(AsSb)/GaAs quantum dots on GaP(001)*.

White Rose Research Online URL for this paper:
https://eprints.whiterose.ac.uk/179827/

Version: Published Version

Article:

Steindl, P., Sala, E.M., Alén, B. et al. (2 more authors) (2021) On the importance of antimony for temporal evolution of emission from self-assembled (InGa)(AsSb)/GaAs quantum dots on GaP(001). New Journal of Physics, 23. 103029.

https://doi.org/10.1088/1367-2630/ac2bd6

Reuse

This article is distributed under the terms of the Creative Commons Attribution (CC BY) licence. This licence allows you to distribute, remix, tweak, and build upon the work, even commercially, as long as you credit the authors for the original work. More information and the full terms of the licence here: https://creativecommons.org/licenses/

Takedown

If you consider content in White Rose Research Online to be in breach of UK law, please notify us by emailing eprints@whiterose.ac.uk including the URL of the record and the reason for the withdrawal request.

eprints@whiterose.ac.uk
https://eprints.whiterose.ac.uk/

New Journal of Physics
The open access journal at the forefront of physics

PAPER • OPEN ACCESS

On the importance of antimony for temporal evolution of emission from self-assembled (InGa)(AsSb)/GaAs quantum dots on GaP(001)

To cite this article: Petr Steindl *et al* 2021 *New J. Phys.* **23** 103029

View the article online for updates and enhancements.

You may also like

- Interfacing quantum emitters with propagating surface acoustic waves
Matthias Weiß and Hubert J Krenner

- Supplementary data

- Charge carrier relaxation in InGaAs-GaAs quantum wire modulation-doped heterostructures
S V Kondratenko, S A Iliash, Yu I Mazur et al.

This content was downloaded from IP address 81.136.47.222 on 01/11/2021 at 11:44

New Journal of Physics
The open access journal at the forefront of physics

Published in partnership with: Deutsche Physikalische Gesellschaft and the Institute of Physics

OPEN ACCESS

RECEIVED
19 July 2021

REVISED
22 September 2021

ACCEPTED FOR PUBLICATION
30 September 2021

PUBLISHED
21 October 2021

Original content from this work may be used under the terms of the Creative Commons Attribution 4.0 licence.

Any further distribution of this work must maintain attribution to the author(s) and the title of the work, journal citation and DOI.

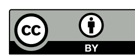

PAPER

On the importance of antimony for temporal evolution of emission from self-assembled (InGa) (AsSb)/GaAs quantum dots on GaP(001)

Petr Steindl[1,2], **Elisa Maddalena Sala**[3,4], **Benito Alén**[5], **Dieter Bimberg**[3,6] and **Petr Klenovský**[1,7,*]

[1] Department of Condensed Matter Physics, Faculty of Science, Masaryk University, Kotlářská 267/2, 61137 Brno, Czech Republic
[2] Huygens-Kamerlingh Onnes Laboratory, Leiden University, PO Box 9504, 2300 RA Leiden, The Netherlands
[3] Center for Nanophotonics, Institute for Solid State Physics, Technische Universität Berlin, Hardenbergstr. 36, 10623 Berlin, Germany
[4] EPSRC National Epitaxy Facility, The University of Sheffield, North Campus, Broad Lane, S3 7HQ Sheffield, United Kingdom
[5] Instituto de Micro y Nanotecnología, IMN-CNM, CSIC (CEI UAM+CSIC) Isaac Newton, 8, E-28760, Tres Cantos, Madrid, Spain
[6] 'Bimberg Chinese-German Center for Green Photonics' of the Chinese Academy of Sciences at CIOMP, 13033 Changchun, People's Republic of China
[7] Czech Metrology Institute, Okružní 31, 63800 Brno, Czech Republic
[*] Author to whom any correspondence should be addressed.

E-mail: **klenovsky@physics.muni.cz**

Keywords: III–V semiconductors, quantum dots, photoluminescence, carrier dynamics, lifetimes

Supplementary material for this article is available online

Abstract

Understanding the carrier dynamics of nanostructures is the key for development and optimization of novel semiconductor nano-devices. Here, we study the optical properties and carrier dynamics of (InGa)(AsSb)/GaAs/GaP quantum dots (QDs) by means of non-resonant energy and time-resolved photoluminescence depending on temperature. Studying this material system is fundamental in view of the ongoing implementation of such QDs for nano memory devices. The structures studied in this work include a single QD layer, QDs overgrown by a GaSb capping layer, and solely a GaAs quantum well, respectively. Theoretical analytical models allow to discern the common spectral features around the emission energy of 1.8 eV related to the GaAs quantum well and the GaP substrate. We observe type-I emission from QDs with recombination times between 2 ns and 10 ns, increasing towards lower energies. Moreover, based on the considerable tunability of the QDs depending on Sb incorporation, we suggest their utilization as quantum photonic sources embedded in complementary metal-oxide-semiconductor platforms, due to the feasibility of a nearly defect-free growth of GaP on Si. Finally, our analysis confirms the nature of the pumping power blue-shift of emission originating from the charged-background induced changes of the wavefunction spatial distribution.

1. Introduction

In the last few decades, semiconductor nano-structures as self-assembled III–V quantum dots (QDs) have been investigated due to their wide range of novel physical properties. Such QDs can be employed in a number of different applications, such as active media in semiconductor lasers [1–3], as building blocks for quantum information devices, particularly for quantum repeaters [4–6], as efficient single and entangled photon sources [7–16], including highly-entangled states for quantum computing [17–20], or as nanomemories [21–25]. Among III–V QDs, particularly type-I indirect (InGa) (AsSb)/GaAs QDs embedded in a GaP(001) matrix [26, 27] have recently attracted attention due to their promising use as storage units for the QD-flash nanomemory cells [26, 27], as potentially effective entangled photon sources [28], owing to their smaller fine-structure splitting (FSS) of the ground state exciton compared to well-known type-I systems such as (InGa)As/GaAs [13, 14], and as quantum gates [28–31]. The concept of

© 2021 The Author(s). Published by IOP Publishing Ltd on behalf of the Institute of Physics and Deutsche Physikalische Gesellschaft

hole storage QD-flash was initially suggested by Bimberg and co-workers [21–25, 32] following first pioneering studies [32] regarding the mechanisms of electron escape from InAs/GaAs QDs, by using the deep level transient spectroscopy. The key feature of the QD-flash is to combine the fast access times of dynamic random access memories with the non-volatility of the flash, which leads to a universal memory type, potentially simplifying future computer architectures. Recently, type-I indirect (InGa)(AsSb)/GaAs/GaP QDs showed an improvement of one order of magnitude in the storage time compared to pure $In_{0.5}Ga_{0.5}As$/GaAs/GaP QDs [33, 34], reaching ∼1 h at room temperature [26, 27]. This result represents to date the experimental record for metal-organic vapor phase epitaxy (MOVPE)-grown QDs, thus opening up the possibility to use this technique to fabricate memory devices based on high-quality III–V semiconductor QDs. The storage time can be increased by further systematic growth parameter optimization of the Sb/P-based type II system, up to the non-volatile regime with storage times exceeding 10 years [35]. Additionally, in reference [28] the authors theoretically discussed the physical properties of such material system—particularly the quantum confinement type—depending on the relative In/Ga and As/Sb contents in the QDs. It was found that these QDs showed concurrently both direct and indirect optical transitions for increasing Sb content, finally leading to type-II band alignment [28]. That made such QDs be excellent candidates for quantum information technologies. Increasing the Sb content in the QDs has been previously made possible by overgrowing (InGa) (AsSb)/GaAs/GaP QDs with a GaSb capping layer, which has effectively modified the QD composition [36]. Moreover, through detailed investigations of their optical properties, it was found that such procedure led to an energy swapping of the Γ and L states, thereby increasing the wavefunction leakage outside the QDs [28, 36]. This property is indeed very appealing for further improvement of storage times since an increased Sb incorporation into the QDs leads to increased hole localization energy [24, 25, 28]. Finally, fabricating QDs on GaP substrates is advantageous in terms of integration on silicon platforms, since the lattice mismatch between GaP and Si amounts to just 0.4%, thus making defect-free MOVPE growth of GaP on Si possible [37].

In this work, we study the carrier dynamics of (InGa) (AsSb)/GaAs/GaP QDs by means of time-resolved-photoluminescence (TRPL) for varying detection energy and sample temperature. This allows us to better separate the spectrally overlapping optical transitions previously observed in our recent work [36]. First, we provide a brief overview of our sample structures. Afterwards, we discuss the experimental results on carrier lifetimes for varying measurement conditions. Analytical models, describing the observed physical phenomena are provided, leading us to discern the different types of optical transitions involved. We would like to point out that, to date, there is no such detailed optical investigation on this material system. Finally, we discuss the material structure in the context of quantum technology applications and comment on the current experimental limitations.

2. Sample structures

The samples were grown by MOVPE in Stranski–Krastanov (SK) mode on GaP(001) substrates at the TU Berlin [26, 27]. The structures of the samples studied in the present work are schematically depicted in all figures as insets.

All samples include 5 Ml-thick GaAs interlayer (IL), a crucial ingredient for the subsequent QD formation, as pointed out by Sala *et al* [26, 38]. The sample having the IL only is referred to as $S_{w/o}$, that labeled S_{with} (S_{cap}) contains (InGa) (AsSb) QDs, without (with) ∼1 Ml GaSb capping. The QDs of density approximately 1×10^{11} cm^{-2} are of truncated pyramid shape, with basis diameter of ∼15 nm and height of 2.5 ± 0.4 nm [26, 28, 36, 39] and were grown with 1 s Sb-flush triggering QDs surface passivation by As–Sb exchange, leading to a decreased tendency of defect formation during their formation [38]. For detailed information about the growth procedure, see references [26, 27, 36]. Additional details on their structure, particularly on size, shape, and composition, can be found in very recent work on XSTM and atom probe tomography investigations on such QD samples [39].

The sample photoluminescence (PL) is found at ∼1.8 eV and shows several not well spectrally separated bands, representing a combination of momentum direct and indirect type-I transitions from QDs [36], visualized in band-scheme diagrams in figure 1 calculated by eight-band $\mathbf{k} \cdot \mathbf{p}$ method using NEXTNANO++ simulation suite [40, 41]. For more information about calculations, we refer to detail theoretical study of electronic states of this material system provided in reference [28].

3. Experimental setup for TRPL measurements

To populate the whole structure with carriers and thus study their dynamics, TRPL experiments were carried out with a pulsed laser with the wavelength of 405 nm, focussed on 0.06 mm^2 area with a 60 ps

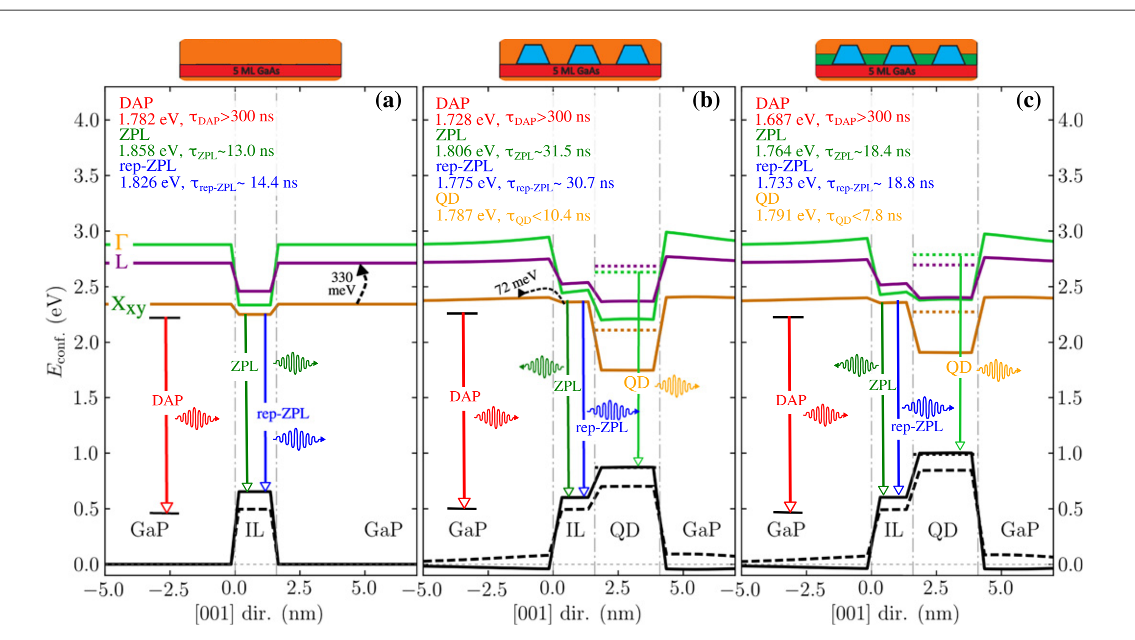

Figure 1. Cross-section along growth direction obtained by NEXTNANO++ [40] simulation of band schemes including eigenenergies indicated by dotted lines for samples (a) $S_{\mathrm{w/o}}$, (b) S_{with}, and (c) S_{cap}. The insets show the experimentally observed recombination times τ_i (i corresponds to recombination origin, see text), transition (taken from fits of PL in the time domain, solid lines) and escape (dashed line) energies derived later in the text. Light (lh) and heavy hole (hh) splitting of valance band are indicated by different line styles (lh: dashed, hh: solid).

pulse-width. The emitted PL spectrum was dispersed by 1200 grooves/mm ruled grating and detected around 1.8 eV by a Si avalanche photodiode. First, we cooled the samples to 15 K, and detected in 200 ns temporal window the energy-resolved TRPL signal for each wavelength. Then, within temperature-resolved TRPL, the sample temperature T was varied in the range 15–130 K. Here, the temporal window was modified to maximize the resolution from 200 ns for lower T, to 25 ns for higher T. Changing the temporal window is connected with changes in repetition rate, which was varied between 5 MHz (for the temporal window 200 ns; used also for energy-resolved TRPL) and 80 MHz (for 25 ns).

4. Spectral line-shape model

For the description of macro-PL in the time domain (TDPL), we take advantage of the similarity in the grown structures, leading to expected shared spectral features across samples associated with carriers confined in the GaAs IL, i.e. zero-phonon (ZPL) and phonon-replica (rep-ZPL) transitions of electrons from X_{xy} conduction minima to Γ valence band maximum [36, 43]. Through analysis of the line-shape in the $S_{\mathrm{w/o}}$ sample, we conclude that the convolution of two asymmetrical bands with maximum emission energy E_{max} concurrently showing a small high-energy and a prominent low-energy band-tail produce better results than the purely Gaussian spectral deconvolution used in reference [36]. The low energy tail shall be related to carrier localization into long-range IL potential fluctuations [44]. Meanwhile, high energy tails shall be related to phonon-assisted thermal population of delocalized states, especially at large excitation powers/temperatures or during the initial stages of the relaxation process. We follow the work of Almosni *et al* to describe the low energy tail long-range fluctuations through the following equation [44]

$$I \propto \frac{\exp(\epsilon/E_{\mathrm{long}})}{E_{\mathrm{long}}} \exp(-\exp(\epsilon/E_{\mathrm{long}})), \tag{1}$$

where a single parameter E_{long} characterizes the long-range potential disorder energy. Meanwhile, hot carrier population is taken into account through an n phonon-assisted thermalization process by line-shape [45]

$$I_n \propto \epsilon^{5/2-n} \exp\left(-\frac{\epsilon}{k_{\mathrm{B}}T_{\mathrm{ca}}}\right) \tag{2}$$

with carrier thermalization energy of $k_{\mathrm{B}}T_{\mathrm{ca}}$; $\epsilon = E - E_{\mathrm{max}}$. We limit our description of I_{IL} (convolution of equations (1) and (2)) to one-phonon process ($n = 1$) only.

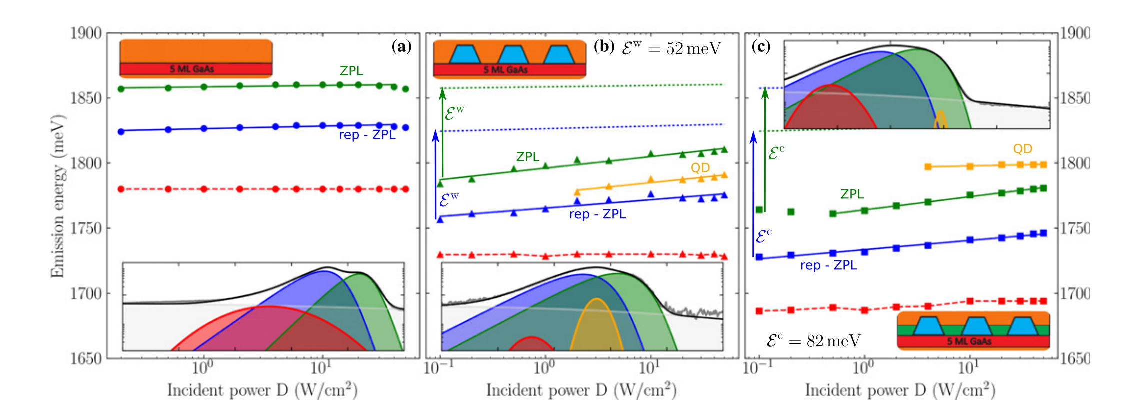

Figure 2. Excitation power dependence of emission energies of samples (a) $S_{w/o}$, (b) S_{with}, and (c) S_{cap}. Symbols represent the emission energies fitted from steady-state PL spectra. A typical (normalized) spectrum of each sample measured with $D = 3.3$ W cm^{-2} together with colored band-reconstruction over spectral range of 1650–1900 meV is shown in insets (semi-logarithmic scale). The emission energies evolve in agreement with diffuse interface model for spatial type-I transitions [36, 42] (solid lines). Low-power emission energies of IL transitions in S_{with} (S_{cap}) are red-shifted by $\mathcal{E}^{w}$ ($\mathcal{E}^{c}$) in respect to that in $S_{w/o}$.

5. Excitation power resolved steady-state PL

Before moving to time-resolved analysis, we show in figure 2 the validity of the fitting model by applying it to the steady-state PL vs continuous-wave excitation power dependence D measured at 15 K and published in our previous study [36]. As it can be seen in figure 2, two replicas of the above lineshape model account for most of the PL emission in these samples, yet not completely. To describe the full PL spectrum, two additional Gaussian profiles are necessary, consistent with continuous-wave macro-PL experiment resolved by excitation power, polarization and sample temperature [36]. One of them describes a rather broad band (FWHM larger than 35 meV), clearly observable only at very low excitation powers, likely originating in the donor-acceptor pair (DAP) transitions in GaP [46, 47] or other defect induced during GaAs IL and QDs formation (the latter in the case of samples with QDs). We attribute the second Gaussian band to the recombination from QDs, being due to non-optimized excitation wavelength, and thus very weak and observable mainly for high excitation powers.

Similarly as there, the fitted peak energies are used to analyse the emission blue-shift with increasing D, in order to determine the type of carrier spatial confinement. Although elsewhere in the literature [48–52] the presence of blue-shift is automatically assigned to indirect spatial alignment, the so-called type-II, we examine here the blue-shift by $E = E_0 + U\ln(D) + \beta D^{1/3}$ [36, 42] allowing us to disentangle type-II band-bending, due to state squeezing represented by the parameter β, from the spatial alignment independent blue-shift caused by crystalline defects described by the Urbach energy tail U. Having β negligible, the analysis in figure 2 suggests that the emission bands of our heterostructures are of type-I, i.e. spatially direct, as also previously reported based on Gaussian fits [36] and in agreement with $\mathbf{k}\cdot\mathbf{p}$ simulations [28]. Moreover, we observe that ZPL and rep-ZPL transitions of samples S_{with} and S_{cap} are red-shifted in respect to their energies observed from PL of $S_{w/o}$ by $\mathcal{E}^{w} = 52$ meV and $\mathcal{E}^{c} = 82$ meV, respectively. This shift partially reflects the strain-relaxation initialized by constituent segregation from QD-layer [39] and, thus, partially induced change in band confinement. The former is connected also with the natural spectral broadening when additional localized defect states are created in the heterostructure. These additional states then form an effective background potential increasing with excitation power, leading to the energy blue-shift of bands of samples with QDs, characterized by the Urbach energy. However, the bands of the sample with only GaAs IL do not manifest blueshift themselves. A similar shift can be also observed in the time domain after the non-resonant pulse-excitation when the carriers first thermalize into the trap states and form the initial background potential. As those recombine, E_{long} decreases, the potential weakens and, thus, the emission energy is gradually red-shifted, as we will discuss later in more detail. This potential weakening is connected also with the spreading of the state wavefunctions, effectively observable as an increase in recombination times in the excitation resolved TRPL, see supplemental information (https://stacks.iop.org/NJP/23/103029/mmedia) [53].

Although we attribute the QD band in the emission of samples with dots, we expect, in the studied spectral range, even richer spectral response related to momentum-indirect transitions of QDs [28] and their compositional variations [39]. These are most likely shadowed by much stronger GaAs IL emission which in comparison with QDs having 3D quantum confinement provides much more states for the

population. To reveal those in future studies, micro-PL experiments with pre-optimized excitation wavelength will be necessary.

6. Emission energy dependent TRPL

In this section, we study the energy-resolved carrier dynamics in our heterostructures by TRPL. To assign the recombination times to the characteristic bands, we first fit the signal (see raw experimental data in figure 3) in individual time bins by the spectral shape model discussed in the previous part, and we refer to this analysis as time-domain PL (TDPL). For the best-fit results presented in figure 4, we use the parameters obtained from steady-state excitation power dependency. Later, we analyse the signal for each wavelength also by the double mono-exponential model (2ME)

$$I(t) = A_1\ \exp(-t/\tau_1) + A_2\ \exp(-t/\tau_2), \tag{3}$$

characterized by amplitude A_1 (A_2) and decay time τ_1 (τ_2) for the slow (fast) decay process. In the case of samples with QDs, we added to the analysis also the third exponential decay component (τ_3), representing the electron–hole recombination in QDs. Typical TRPL deconvolution to individual decay channels for each sample taken at the PL maximum is shown in figures 3(d)–(f); extracted time constants qualitatively agree with TDPL analysis. Finally, we analyze the spectral distribution of the time decay constants τ_1–τ_3 by an analytical model developed by Gourdon and Lavallard [54]:

$$\tau = \frac{\tau_r}{1 + \exp[(E - E_{me})/U_0]} \tag{4}$$

which is widely used in the literature [55, 56], even though in equation (4) the hopping processes [54] or temperature dependence [57] are not included. The meaning of the parameters in equation (4) is as follows: τ_r is the exciton radiative lifetime, E_{me} the characteristic energy for which the radiative time equals the transfer one, analogously to a mobility edge [56, 58], and U_0 is the measured energy of localized states, similar to Urbach energy tail, responsible for the observed energy blue-shift [42]. Note, that τ_1 process decays rather slowly and does not completely disappear in one temporal window, therefore we take into account its repumping from previous pulses in TRPL fits, as discussed in the appendix. This issue is overcome in TDPL by disentangling individual transitions by line-shape model fitting, where the slowest decay is assigned to (mainly non-radiative) pair recombination of DAP in GaP [46, 47]. Moreover, in spectral dependence for the evaluation of τ_1 we need to extend the model (4) by an additional contribution, likely connected with other defects created during the epitaxial growth process.

Note, that we do not assume effects such as dark excitons of QDs and dark states in general as well, which are typically much weaker than bright-state QD emission, particularly in macro-PL of samples with a non-optimized excitation wavelength and a large spectral overlap of transitions. These effects can become observable and more information about the structure dynamics can be gained if only few QDs are isolated, either by near-field optical methods or in micro-PL experiments, ideally with more efficient optical addressing of the QD area by excitation laser closer to the energy of the transitions ($\sim$ 1.8 eV), yet below deep level resonances in GaP (approx. 2.2 eV) [47] to minimize absorption in substrate, or by optical pumping of the wetting layer [59, 60].

6.1. Sample without QDs $S_{w/o}$

We start our discussion with the sample $S_{w/o}$. TDPL deconvolution allows us to study not only the relaxation-time constants of the considered decay process but also the energy changes of the state in the time domain. Specifically, the emptying of the impurity states entails an exponential-like decrease of the emission energies of the total energy ΔE for both ZPL and rep-ZPL bands, also recently observed for relaxed GaAs/GaP QDs with type-I band-alignment [61]:

$$E(t) = E_0 + \Delta E\ \exp(-t/\tau_E), \tag{5}$$

where $E_0 + \Delta E$ is the energy of the observed state after laser excitation, which exponentially decays proportionally to the time constant τ_E (an effective time when impurities and defects affect the electron state) to electron energy E_0. That can be equally well understood as due to defects at the interfaces between segments of the heterostructure, which create a local electric field (non-equilibrium carriers) leading to red-shift ΔE of the electron state with energy E_0. The carriers then recombine for τ_E upon which the eigenvalue of electron state returns to its value without the presence of the local field E_0. Note, that the shift ΔE cannot be caused by inter-valley scattering, which is three orders of magnitude faster than the observed τ_E [62, 63], nor by the thermalization of higher excited states (since $\tau_E >$ radiative recombination times) or

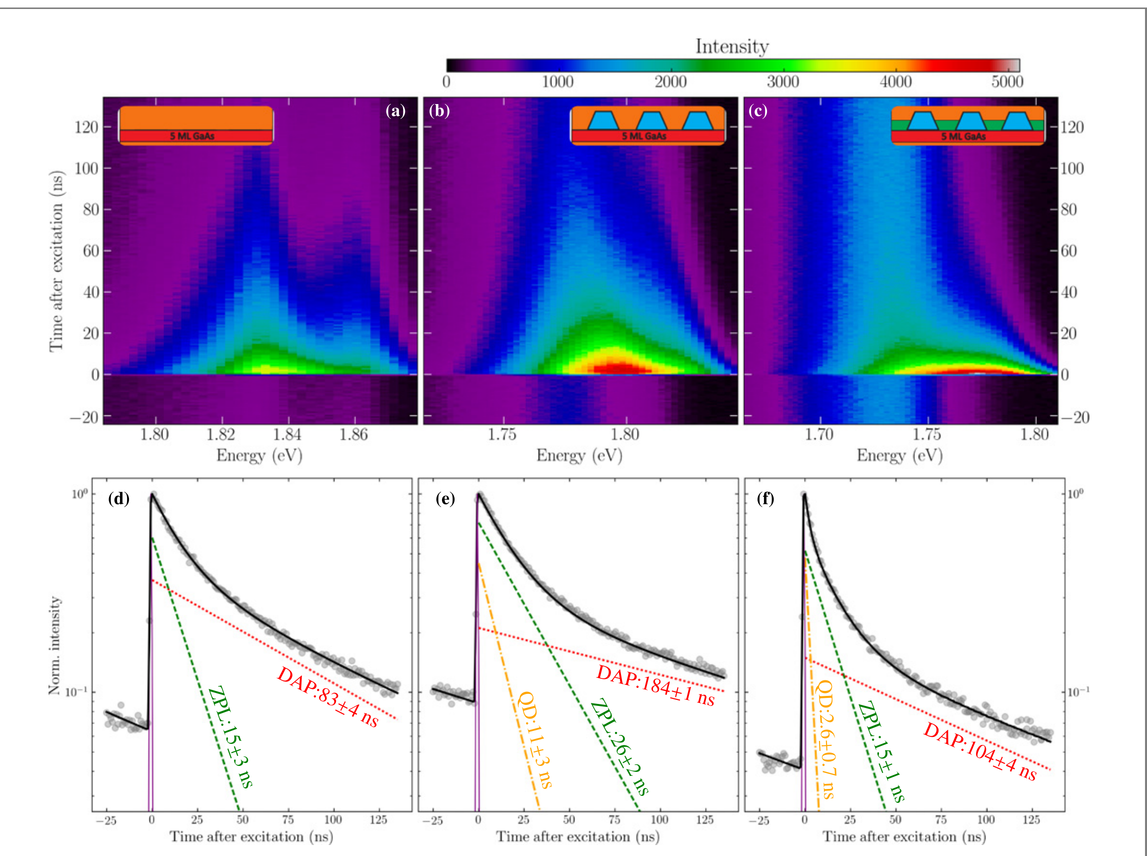

Figure 3. False-color plots of PL intensity as a function of time and emission energy for samples (a) $S_{w/o}$, (b) S_{with}, and (c) S_{cap}. The color scale is identical for all samples. Deconvolution of TRPL signal to individual channels taken at PL maximum of the sample: (d) $S_{w/o}$ at 1.84 eV, (e) S_{with} at 1.80 eV, and (f) S_{cap} at 1.77 eV. The fit (solid black line) of experimental data (gray symbols) includes Gaussian pulse detector response (purple), background of 50 counts (not shown), and 2 or 3 exponential decays distinguished by color (QD: orange dash–dotted; ZPL: green dashed; DAP: red dotted) including repumping.

thermalization of free-carrier created after excitation which is of one order of magnitude faster, see T_{ca} in supplemental information [53].

Even though both bands are shifted by few units of meV, similarly to the total blue-shift observed in steady-state experiments, the integral TDPL spectrum taken at different times of measurement does not show any significant shift and decays equally in time proportionally to the decay around 10–15 ns, see inset of figure 4(a) and table 1. Note, that since for the studied samples the energy level separations of IL, DAP, and QDs are not clearly distinguishable, we use double mono-exponential decay function (with time constants τ_1^{TDPL} and τ_2^{TDPL}) to deconvolute the emission intensity, where the origin of the second time constant is assigned according to the following: DAP and other non-radiative defects decay slowly ($\tau_2^{\mathrm{TDPL}} > 40$ ns), whereas QD transition is fast ($\tau_2^{\mathrm{TDPL}} < 10$ ns).

The standard TRPL deconvolution at each wavelength in figure 5(a) shows two contributions. The faster, being in good agreement with ZPL and rep-ZPL TDPL band decays, with time constants around 13 ns contributes more or less constantly by 20% to the total intensity (panel (b)). The slower process, related to DAP and crystalline defects, increases the time-constant up to $\sim$ 200 ns towards lower energies where none transition from GaAs IL is expected [28, 43] and is saturated below 1.79 eV as expected from the similarity with the two other samples. Note, that similar behaviour with extremely slow (up to few μs) low-energy transition were independently reported for (In, Ga)As/GaP [64, 65], Ga(As,P)/GaP [66], and GaSb/GaP [67] as momentum-indirect transitions from QDs. Because we observe such transition not only for our QDs with completely different stoichiometry but also for GaAs/GaP sample clearly without any QDs, we tend to assign the slow transition to defects in GaP substrate [68, 69], common for all reported structures. Furthermore, we note in figure 5(a) a good agreement between TDPL and TRPL time constants, allowing us to deduce, in power and temperature resolved experiments, the character of relaxation based on the results of TRPL measurements only.

6.2. Sample with QDs S_{with}

The whole spectrum of S_{with} (figure 3(b)), including ZPL and rep-ZPL bands, is also red-shifted in TDPL in respect to that of $S_{w/o}$, approximately by $\mathcal{E}^{w}$, see figure 4(b) and table 2. That is close to the energy shift of

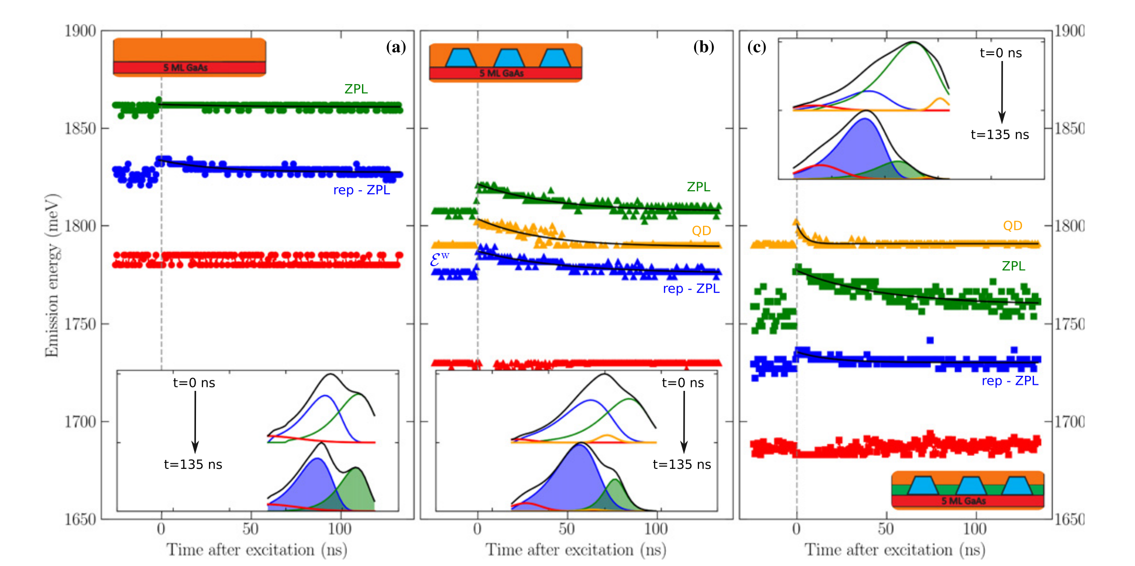

Figure 4. Fitted TDPL emission energies (symbols) which exhibit exponential-like energy red-shift with temporal evolution (fit, black solid lines). While for $S_{w/o}$ in (a), the shift is timid, for samples S_{with} (b) and S_{cap} (c) it exceeds 10 meV and leads to an observable spectral-shape variation within temporal evolution (see panels (a)–(c) of figure 3 and emission energy shift of the spectra in insets with color-coded fitted emission bands across the spectral range of 1.65–1.9 eV at $t = 0$ and after 135 ns). The broken grey vertical lines indicate the moment of the laser pulse excitation ($t = 0$ in insets).

Table 1. Summary of the best-fit parameters of the spectral shape model applied to the excitation power resolved PL and TDPL of all studied samples. Symbol * (**) refers to a discrepancy of +10 meV (−5 meV) in E_0 from TDPL in respect to the extracted value from the excitation power-dependent PL. For QDs, we give FWHM as E_{long}.

Sample	Transition	E_{long} (meV)	E_0 (meV)	U (meV)	ΔE (meV)	τ_E (ns)	τ_1^{TDPL} (ns)	τ_2^{TDPL} (ns)
	ZPL	10	1858 ± 0.4	0.5 ± 0.2	1.3 ± 0.4	50 ± 40	10.7 ± 0.2	52 ± 1
$S_{w/o}$	Rep-ZPL	14	1826 ± 0.4	0.8 ± 0.1	5.9 ± 0.4	31 ± 5	11 ± 3	87.6 ± 0.7
	ZPL	19	$1796^* \pm 1$	3.9 ± 0.4	13.8 ± 0.5	41 ± 4	6.8 ± 0.1	47 ± 1
S_{with}	Rep-ZPL	20	$1765^* \pm 1$	2.8 ± 0.4	11 ± 1	46 ± 6	12.9 ± 0.5	47 ± 1
	QDs	19	$1777^* \pm 2$	3.6 ± 0.6	14.3 ± 0.5	35 ± 4	10.4 ± 0.1	
	ZPL	20	1764 ± 0.4	4.4 ± 0.1	17 ± 1	44 ± 7	14.9 ± 0.1	2.0 ± 0.1
S_{cap}	Rep-ZPL	23	1733 ± 0.4	3.1 ± 0.2	5.4 ± 0.7	19 ± 4	68 ± 4	
	QDs	8	$1796^{**} \pm 0.6$	0.7 ± 0.2	10 ± 1	4.1 ± 0.4	7.7 ± 2	

$E_{me}(S_{w/o}) - E_{me}(S_{with}) = 47$ meV for ZPL (55 meV for rep-ZPL) and together with similar time constants τ_1^{TDPL}, pointing to similar physics behind the I_{IL} transitions. The best fit emission energies of ZPL and rep-ZPL after excitation show non-equilibrium carrier background potential, initially squeezing the electron wavefunction [48, 70]. Later, as the potential weakens, the wavefunction spatially spreads, leading to the gradual red-shift ΔE of 14 meV and 11 meV for ZPL and rep-ZPL bands, respectively, to their steady-state energies. This time, in agreement with large blue-shift in excitation power-dependent PL, the shifts are more prominent due to significantly increased number of defects created within QD layer formation and later due to additional atom segregation [39]. In addition to the sample $S_{w/o}$, we observe also ΔE of 14 meV for the TDPL QD band with time constant of ~10 ns, suggesting impurity induced dynamics connected with the GaAs layer.

The TRPL signal, deconvoluted by equation (3) by three mono-exponential decay contributions, shows two patterns: one similar to that observed for $S_{w/o}$, and also a much faster one, which we attribute to the emission from QDs. These processes, depicted in panels (c) and (d) of figure 5, have different weight $[w_i = A_i\tau_i/(\sum_j^3 A_j\tau_j)]$ across the measured spectral range. While for energies below 1.75 eV the DAP dynamical processes dominate in weight, they lose importance for larger energies in favor to the processes involving the GaAs IL. The QD contributions are almost negligible in weight in the whole spectral range, except for an increase of w_3, corresponding to QDs, centered around 1.80 eV and 1.83 eV, where w_3 is larger than 10%. The mean values of τ_3 in these spectral ranges are 9.0 ± 1.0 ns and 6.0 ± 1.0 ns, respectively. Note that we cannot find any conclusion about the QD transition brightness purely from its weight, since its value is affected by the recombination times of transitions which QDs are compared with—in our case decay times of up to two orders magnitude higher than QDs. On the other hand, the TRPL deconvolution in figure 3 and also fit of TDPL data in inset of figure 4 fully reveal the contribution to

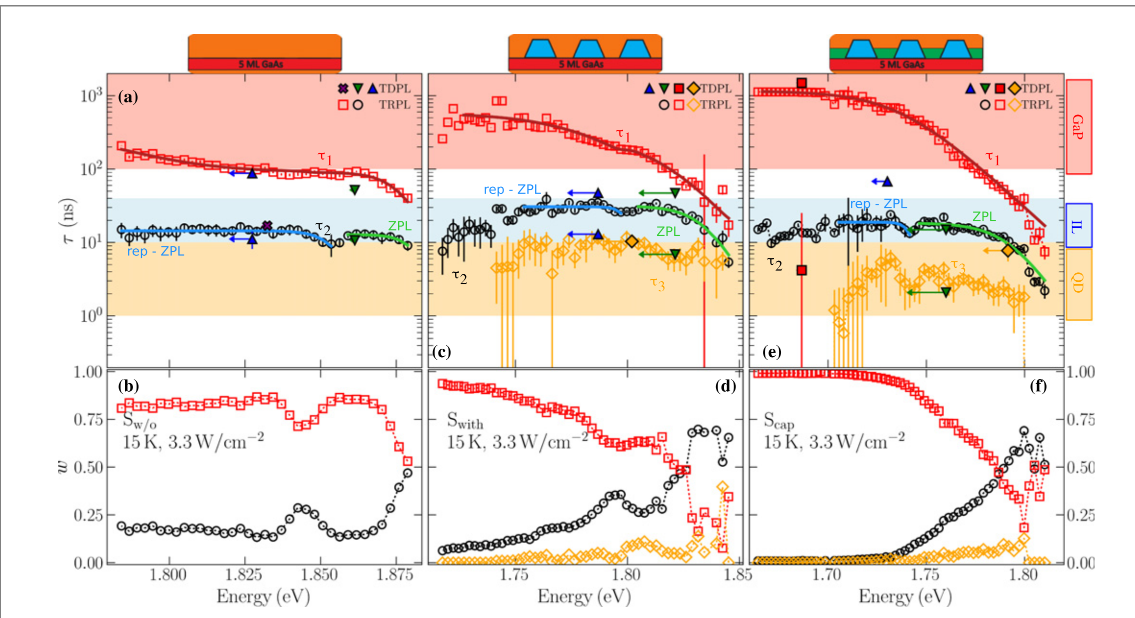

Figure 5. The energy dispersion of (a) time constants and (b) corresponding weights w [$w_i = A_i\tau_i/(\sum_j^{j_{\max}} A_j\tau_j)$, $j_{\max} = 2(3)$ for 2ME (3ME) fitting model] for sample $S_{w/o}$ obtained by fitting the TRPL signal by the double mono-exponential model using equation (3) (symbols) and fitted by the Gourdon–Lavallard's model (4) (solid lines) [54]. That for samples S_{with} and S_{cap} obtained from fitting of the TRPL signal by triple mono-exponential model using equation (3) is shown in panels ((c) and (d)) and ((e) and (f)), respectively. The deconvoluted time constants show good agreement with TDPL intensity decays (full symbols with arrows representing time-domain ΔE shift; transitions are assigned by color in agreement with figure 4). Shaded areas of 1–10 ns, 10–40 ns, and > 100 ns correspond to different recombination channels.

Table 2. Parameters obtained from Gourdon and Lavallard model, equation (4). Units of the variables are: τ_r^i is in ns, E_{me}^i and U_0^i are in meV.

	GaAs IL			GaAs IL, phonon rep.		
Sample	τ_r^{ZPL}	E_{me}^{ZPL}	U_0^{ZPL}	τ_r^{rep}	E_{me}^{rep}	U_0^{rep}
$S_{w/o}$	13.0 ± 1.0	1882 ± 3	4 ± 2	14.4 ± 2.4	1856 ± 2	4.3 ± 1.4
S_{with}	31.5 ± 0.7	1835 ± 1	8.0 ± 0.6	30.7 ± 0.3	1801 ± 2	2.7 ± 1.1
S_{cap}	18.4 ± 0.5	1792 ± 1	11 ± 1	18.8 ± 0.3	1743 ± 1	2.5 ± 0.9
	Growth defects			DAP in GaP		
Sample	τ_r^{d}	E_{me}^{d}	U_0^{d}	τ_r^{DAP}	E_{me}^{DAP}	U_0^{DAP}
$S_{w/o}$	90 ± 1	1877 ± 1	5.3 ± 0.2	260 ± 30	1776 ± 3	15.6 ± 0.5
S_{with}	284 ± 2	1810 ± 1	14.9 ± 0.1	561 ± 1	1781 ± 1	17.0 ± 0.1
S_{cap}				1156 ± 1	1737 ± 1	17.6 ± 0.2

the signal, which is prominent few nanoseconds after excitation when it clearly exceeds concurrent DAP recombination, even though $w_3 \approx 10\%$.

For the spectral characteristic of the transitions, the Gourdon and Lavallard model [54] was used by means of one contribution for the process τ_2, and two contributions for the process τ_1. The best-fit values (see table 2) show the mobility edge of the ZPL transition in IL shifted with respect to that of $S_{w/o}$ by 47 meV, which is in the agreement with the shift of the whole spectrum discussed previously. On the other hand, the mobility edge of DAP in GaP remains not affected by the heterostructure. The radiative time of the ZPL (rep-ZPL) band is 31.5 ± 0.7 ns (30.7 ± 0.3 ns), which is more than two times larger than that of the sample without QDs. That increase can be understood in terms of different material distribution, as an effect of strain relaxation discussed in [36] due to the GaAs IL overgrowth with QDs, leading to the change of the confinement potentials. On the other hand, disorder energies U_0 originating from material redistribution—in our case mainly due to the strain relaxation—are higher than for $S_{w/o}$, indicating increased disorder of GaAs IL interface.

6.3. Sample with GaSb-capped QDs S_{cap}

As previously shown in [36] by comparison of experimental and $\mathbf{k} \cdot \mathbf{p}$ simulated emission energies, overgrowing the QDs with a thin (~1 Ml) GaSb cap leads to an effective increase of the Sb content in QDs. Through the TDPL analysis of sample S_{cap} using the line-shape model with emission energies and FWHM

adopted from excitation power dependence, we refine the character of the emission band and assign in figure 5 the lifetimes of the observed optical transitions, see particularly the fit in inset of figure 4(c).

Across the studied spectral range, we again observe similar signatures as in $S_{w/o}$, but red-shifted by $\mathcal{E}^c$. This shift is also apparent from the comparison of mobility edges subtracted from the Gourdon and Lavallard model [54], given in table 2. In contrast to the previous samples, we observe also 40 meV shift of DAP mobility edge which is a rather significant change to be caused by a different character of the DAP process only (i.e. type, or concentration) and possibly causing much longer rep-ZPL transition time as extracted from TDPL. However, we do not observe any change of the mobility edge for samples $S_{w/o}$ and S_{with}: this might be still connected to the effect of layer-overgrowth on dynamics. On the other hand, we observe almost unchanged ZPL radiative time of 16.2 ± 0.2 ns (and 14.9 ± 0.1 ns from TDPL).

The whole emission spectrum in figures 3(c) and 4(c) shows changes in the shape of emission bands in the time domain, including observable spectrum red-shift. From TRPL deconvolution by three mono-exponential decay curves, it can be seen that the spectrum consists of the fast component at energies greater than 1.75 eV, which completely disappears during the first 50 ns after excitation, and it is rapidly red-shifted during that period. After 50 ns, only a part of the band at energies below 1.75 eV remains bright. In agreement with the observations for S_{with}, below 1.74 eV the DAP dynamical processes clearly dominate and their time constant is $\sim$1 μs. For larger energies, the emission due to DAP loses importance in favor of GaAs IL processes. For energies larger than 1.76 eV, also the contribution of QDs starts to be noticeable with $w_3 \sim 10\%$ and τ_3 of 2–6 ns.

The time-evolution of the best-fit emission energies of individual transitions from the TDPL fit given in figure 4(c) shows that ZPL and rep-ZPL bands are exponentially red-shifted by 17 meV and 5 meV, respectively, with time constant τ_E being 19–44 ns.

The previous analysis showed an increase of QD recombination times with decreasing energy from 6 ns to 9 ns for S_{with}, of 1.83 eV and 1.80 eV, respectively, and from 2 ns to 6 ns for S_{cap} of energies close to 1.79 eV and 1.73 eV. Thus variations in recombination times shall be attributed to statistical fluctuations of the confinement potentials. Also here, single dot spectroscopic study [71] will be beneficial to eliminate ensemble averaging [72] and potentially reveal also dynamics of much slower indirect and/or dark transitions.

7. Temperature dependent TRPL

In this section, we separate radiative (τ_R) and non-radiative (τ_{NR}) contributions of the observed decay times and complete the band schemes in figure 1 of the observed non-radiative processes. Individual recombination channels as a function of T were extracted again using the 3ME (2ME) model for deconvolution of TRPL signal of S_{with} and S_{cap} ($S_{w/o}$). Contrary to the sample $S_{w/o}$, the decay time of ZPL (τ_2) for samples with QDs (S_{with} and S_{cap}) increases with T between 30 and 50 K and thereafter progressively reduces, which is characteristic for the activation of thermally activated escape paths of shallow defects [73]. Those are most likely generated at the IL/QDs interface during the strain-relaxation caused by QDs overgrowth [36].

Neglecting dark states being under resolution of our experiments, we assume, in accordance with reference [74], that at 15 K the dominant loss mechanism is the radiative recombination. Thereafter, $\tau_{R,j}$ and $\tau_{NR,j}$ decay times can be estimated from the decay time of τ_j by [75, 76]

$$\tau_{R,j} = \frac{I_0}{I_{PL}(T)}\tau_j, \tag{6}$$

and

$$\frac{1}{\tau_j} = \frac{1}{\tau_{R,j}} + \frac{1}{\tau_{NR,j}}, \tag{7}$$

where I_0 and I_{PL} are the PL intensities integrated at PL maximum at 15 K and at larger T, respectively. Thermally activated scattering processes cause an exponential decrease of $I_{PL}(T)$ with rising temperature (shown in the supplementary material), characterized by τ_{NR} of localized carriers with T. That process can be quantitatively interpreted by the model involving up to two non-radiative thermal-activation processes [76]

$$\frac{1}{\tau_{NR,j}} = \frac{1}{\tau_{NR}^1}\exp\left(\frac{-E_1}{k_B T}\right) + \frac{1}{\tau_{NR}^2}\exp\left(\frac{-E_2}{k_B T}\right), \tag{8}$$

Table 3. Summary of the parameters from temperature TRPL deconvolution.

Sample	Process	E_1 (meV)	E_2 (meV)	τ_R^0 (ns)	τ_R^T (ns)	T_C (K)
	τ_1	20 ± 1	330 ± 14	65.6 ± 0.5	≈ 0.00	8 ± 2
$S_{w/o}$	τ_2	22 ± 1	305 ± 10	15.1 ± 0.8	0.4 ± 0.3	53 ± 17
	τ_1	4.1 ± 0.4	72 ± 7	108 ± 1	1.9 ± 0.2	26 ± 1
S_{with}	τ_2	7 ± 1	—	18 ± 1	6.9 ± 1.3	57 ± 4
	τ_3	3.4 ± 0.3	—	7.8 ± 1.8	6.9 ± 1.5	63 ± 6
	τ_1	23 ± 1	—	95.5 ± 0.5	≈ 0.00	35 ± 5
S_{cap}	τ_2	23 ± 1	—	12 ± 3	2.8 ± 1.0	43 ± 13
	τ_3	5.3 ± 0.4	—	3.2 ± 1.1	0.12 ± 0.02	14 ± 4

characterised by the activation energies E_1 and E_2 and time constants τ_{NR}^1 and τ_{NR}^2, respectively. Conversely, τ_R of exciton increases exponentially with T [74, 77]

$$\tau_{R,j} = \tau_R^0 + \tau_R^T \left[\exp\left(\frac{T}{T_C}\right) - 1\right], \tag{9}$$

where τ_R^0 (τ_R^T) describes the T independent (dependent) part of the radiative lifetime, and T_C is the characteristic value of T corresponding to the energy of the localised states. Due to implicit dependency of radiative lifetime on the density of interface defects [78], we later use the parameter τ_R^T for qualitative comparison of material redistribution in the samples.

In order to simplify the model, we have neglected any non-radiative recombination at 15 K. The conclusions would not change including the non-radiative recombination at 15 K. The results for the decay times are summarised in table 3 and in supplementary material [53]. The parameters derived from the radiative lifetime of QDs and ZPL are obtained from three free parameter fits with reduced $\overline{\chi}^2$ between 1 and 2. For DAP the fits are worse with $2 < \overline{\chi}^2 < 5.5$. Because the data for non-radiative contributions are based on radiative lifetimes, we observe a worse fit (with either two or four free parameters) quality with $1 < \overline{\chi}^2 < 5.5$ using the non-radiative model equation (8).

We attributed the slowest process τ_1 to the recombination of DAP and other crystalline defects, which follows the same trend with increasing T for $S_{w/o}$ and S_{cap}, i.e. it decreases over 2 orders of magnitude from 100 ns to 1 ns. Due to larger amount of defects, τ_1 of S_{with} decreases only by one order of magnitude up to 20 ns, which significantly changes the character of the radiative lifetime, increasing exponentially [77] with T from $\tau_R^0 = 108 \pm 1$ ns at 15 K due to thermalization of the defects on IL/QDs interface [39]. Comparing $S_{w/o}$ and S_{cap}, we find τ_R to be constant at 65.6 ns and 95.5 ns, respectively. For these two samples, the material intermixing and related generation of thermalization centres is prevented by the absence of QDs and reduced by the capping layer, respectively.

The radiative time constant τ_R of the faster process τ_2 increases exponentially across the samples with T from $\tau_2 \approx 15$ ns. This increase is most likely caused by impurity thermalization via T_C ($T_C \approx 50$ K is close to disorder energy determined for these samples in [36]). While no material exchange in GaAs IL for sample $S_{w/o}$ occurs by design, confirmed by the observation that the amplitude τ_R^T of thermalization change of τ_R is almost zero. After QD formation, In–Ga redistribution between QD and GaAs IL occurs as previously reported in references [36, 39], leading to almost twenty-fold increase of τ_R^T (sample S_{with}). The redistribution can be prevented by overgrowing the structure by a thin GaSb capping layer (see the similarity in panels of S_{cap} and $S_{w/o}$ in figure 6), which for a thickness of ~1 ML leads to approximately six-times larger τ_R^T than that for sample S_{cap}, and an As–Sb intermixing between QDs and capping takes place, resulting in an increase of the Sb content in QDs [36].

It can be assumed that the importance of this effect can be reduced if the Sb layer is thicker because then the capping might be more robust, yet that can also result in pushing the wavefunctions out of the QD body, and the corresponding change of the type of spatial band-alignment, previously reported for similar dots grown on GaAs substrate in references [79–81].

The fastest process τ_3 was considered only for QD samples S_{with} and S_{cap}. The parameter τ_3 of the sample S_{with} decreases from ~ 10 ns (at 15 K) to 6 ns (at 70 K), see figure 6(e). Since the value of the lifetime is close to τ_2, we assume that the electrons are localized preferably at the QD/IL interface. The radiative part τ_R is quenched with $T_C = 63 \pm 6$ K, corresponding to thermalization energy of ≈ 5 meV, which is in good agreement with 4.5 meV, previously extracted from the thermal red shift [36]. The presence of additional Sb during QD formation and ripening, which for S_{cap} would translate into the growth of the GaSb cap right after the QD formation, has very likely led to the formation of smaller and more homogeneous QDs, as a result of the Sb surfactant effect, as also pointed out by Sala *et al* in references [26, 38]. This process could have, thus, led to a better electron-wavefunction localization in the QD body.

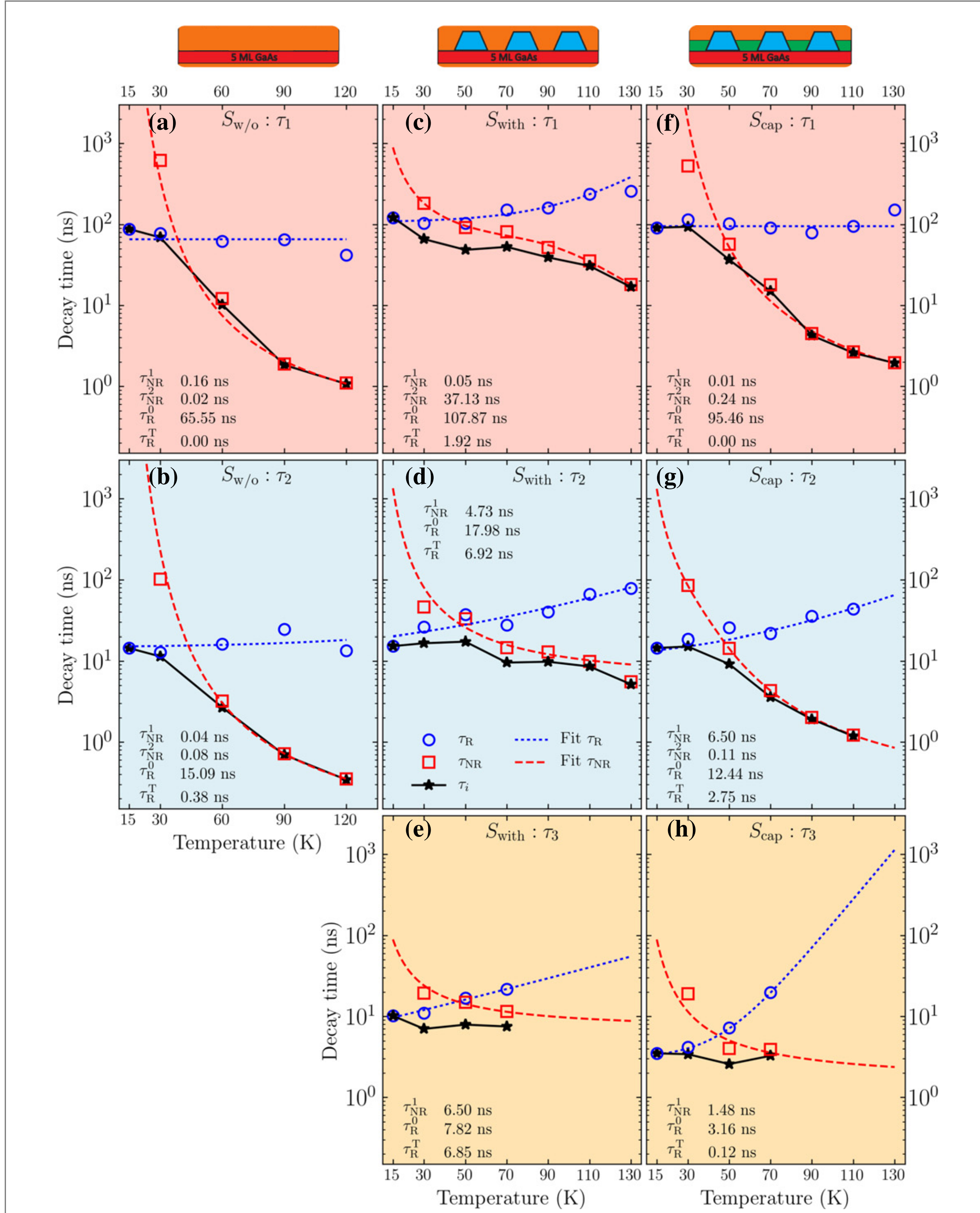

Figure 6. Individual TRPL decay times τ_1–τ_3 (black stars) shown as a function of temperature with the radiative (blue) and non-radiative (red) components for all three samples-panels (a) and (b) show decay times for sample $S_{w/o}$, (c)–(e) that for S_{with} and (f)–(h) for S_{cap}. The radiative and non-radiative component (circles and squares) are fitted by equations (9) and (8) (broken curves), respectively. The best-fit parameters from the models are added for easier comparison.

The better electron-wavefunction localization results in a shorter decay time τ_3 of $\approx$ 3 ns (at 15 K and decreasing to 2 ns at 70 K), see figure 6(h). This is in agreement with the 2.5 ns observed at 4 K for (InGa)(AsSb)/GaAs/GaP QDs grown with higher Sb flow [38]. This points to the fact that both growing a thin GaSb cap above the QDs and using a higher Sb flow before QD formation are both efficient ways to affect the QD structural properties and possibly increase the Sb content in the QDs [39]. Note, that contrary to pure Sb-flush effect [38] mainly passivizing the surface before QD formation, here we also observe an energy shift of the PL for the sample S_{cap}, most likely a signature of Sb integration into QD body, due to the presence of the GaSb capping layer.

The analysis of non-radiative lifetimes in panels (a) and (b) of figure 6 shows that both PL bands of the sample $S_{w/o}$ are thermally quenched via phonon-excitation from X-valley in GaAs, with activation energy

$E_1 \sim 20$ meV. This activation energy is in good agreement with activation energies of 10–30 meV extracted from steady-state PL [36, 82]. For larger T, PL of the both transitions is quenched via unipolar escape of electrons from X-valley to L-valley in GaP, with activation energies of $E_2 \sim 330$ meV being close to 370 meV predicted with eight-band $\mathbf{k} \cdot \mathbf{p}$ [36].

The non-radiative lifetime analysis of S_{with} transitions, panels (c)–(e) in figure 6, shows that the emission at low temperatures is thermally quenched via electron-thermalization from X_{xy} in IL to, most likely, nitrogen complexes present in the structure from GaP growth [83], with escape energies of 3–7 meV [84]. For larger temperatures, the dominant mechanism of quenching with escape energy 72 ± 7 meV (77 meV observed in steady-state PL [36]) is most likely the escape of electron from X_{xy}-valley in IL to X-valley in bulk. The extracted escape energy is close to the theoretical binding energy of 41 meV determined from eight-band $\mathbf{k} \cdot \mathbf{p}$, and experimentally confirmed value of 43 ± 7 meV [85]. Having lower eigenenergy and many of available electron states, makes the escape from X_{xy}-valley in IL to X-valley in bulk preferable over two concurrently possible paths with similar escape energies—the escape of electron from X_{xy}-valley in IL to L-valley in IL (binding energy 87 meV) and the escape of L-electron in QDs to the bulk GaP (46 meV). Note, that calculating the activation energies by $\mathbf{k} \cdot \mathbf{p}$ model, i.e. without atomistic resolution, cannot explain the observed discrepancy to measured activation energies possibly caused by intermixing and material redistribution on the interface between QDs and GaAs IL. Such created concentration gradient is leading to local strain and potential changes affecting the escape of carriers and, therefore, a slight discrepancy between experiment and simulation is expected.

Repeating the similar analysis on temperature dependency of non-radiative lifetimes of emission from S_{cap} presented in panels (f)–(h) of figure 6, we identify, that the emission from this sample is quenched by shallow impurities (escape energy of 5 meV) and phonon-emission from X-valley in GaAs (≈ 23 meV).

8. Conclusions and outlook

We performed the first detailed analysis of the carrier dynamics of (InGa) (AsSb)/GaAs/GaP QDs to date, by means of energy and temperature modulated TRPL. Based on steady-state PL measurements carried out in our previous work [36] as a reference, we develop spectral shape model taking into account phononic, impurity-related, and thermalization effects to address the four emission bands expected from $\mathbf{k} \cdot \mathbf{p}$ calculations [28]. The application of analytical models shows similarities across the samples studied here, originating from GaAs IL and defects in the GaP substrate. Specifically, the transitions are zero-phonon and phonon-assisted transitions of electrons in the GaAs IL from the X_{xy} valley to the Γ valence band, with decay times around 15 ns, and DAP recombination in GaP decaying extremely slowly (up to few μs). Moreover, we observe type-I emission from QDs, which is faster than 10 ns and its recombination times varies across the studied range, most likely due to coexistence of momentum direct and indirect transitions and compositional changes of individual dots. Finally, we want to point out the spectral shift of the type-I emission from GaAs IL and QDs bands caused by charge potentials from defects created during QD formation. This shift is evident in both pump-power resolved steady-state PL, as well as in the time domain study of the emission.

Our data suggest that epitaxial growth strategies can be employed to efficiently increase the Sb content in the QDs by a thin GaSb cap overgrowth. Such Sb concentration increase in QDs enhances the carrier confinement and could subsequently lead to an increase of the QD storage time, which is of utmost importance for the implementation of such QDs into nano-memory devices [24, 35]. However, the use of Sb, and its potential partial segregation [39, 86], might lead to the formation of additional point defects, which could affect the storage time by increasing capture cross-section [87]. Therefore, the development of the truly defect-free Sb-rich QDs on top of GaP is the key for further improvement of QD-Flash nano-memories. In this respect, further epitaxial engineering techniques are demanded [88]. However, considering the present study and our previous work [36], we have demonstrated that overgrowing such QDs with a GaSb capping layer is a promising epitaxial method to increase the Sb content in (InGa) (AsSb) QDs and to manipulate their carrier dynamics.

Furthermore, for their naturally small FSS [14], such Sb-rich dots are promising candidates for entangled-photon sources, potentially operating not only at cryogenic temperatures due to Sb-increased electron confinement. Their use as entangled-photon, as well as single-photon sources, will require future effort in the optimization of optical efficiency by both sample quality and cavity enhancement [89]. Even though the growth may be challenging, these structures have benefits, such as small size and improved compositional homogeneity compared to conventional SK QDs [26, 27, 39]. Moreover, considering the negligible lattice mismatch between GaP and Si, they can serve as a CMOS compatible quantum platform. Finally, since the incorporation of Sb during growth leads to (i) tunable quantum confinement of the dots

Figure A1. TRPL decay signal with $\tau = 350$ ns (blue for 1st window, red for 2nd) after excitation (black) shown in two consecutive temporal windows (200 ns). Gray symbols represents compound signal from two temporal windows. The arrow points to re-pumped signal from background level (including dark counts) due to contribution to the measured signal from the previous temporal window.

[28] and (ii) the possibility to reduce the amount of charge trap states originating from crystal structure imperfections, we suppose our dots might be superior to those recently proposed on SiGe QDs [90, 91].

Acknowledgments

PS is Brno PhD Talent Scholarship Holder-Funded by the Brno City Municipality and acknowledges funding from the EU Horizon 2020 Programme (GA 862035 QLUSTER). EMS and DB thank the DFG (Contract No. BI284/29-2). A part of the work was carried out under the project CEITEC 2020 (LQ1601) with financial support from the Ministry of Education, Youth and Sports of the Czech Republic under the National Sustainability Programme II. Project CUSPIDOR has received funding from the QuantERA ERA-NET Cofund in Quantum Technologies implemented within the European Union's Horizon 2020 Programme. In addition, this project has received national funding from the MEYS and funding from European Union's Horizon 2020 (2014–2020) research and innovation framework programme under Grant Agreement No. 731473. This project (20IND05 QADeT) has received funding from the EMPIR programme co-financed by the Participating States and from the European Union's Horizon 2020 research and innovation programme. The work reported in this paper was (partially) funded by project EMPIR 20FUN05 SEQUME. This project has received funding from the EMPIR programme co-financed by the Participating States and from the European Union's Horizon 2020 research and innovation programme. The work reported in this paper was (partially) funded by project EMPIR 17FUN06 Siqust. This project has received funding from the EMPIR programme co-financed by the Participating States and from the European Union's Horizon 2020 research and innovation programme. This works was also partially funded by Spanish MICINN under Grant PID2019-106088RB-C31 and by the MSCA-ITN-2020 Funding Scheme from the European Union's Horizon 2020 programme under Grant Agreement ID: 956548.

Data availability statement

The data that support the findings of this study are available upon reasonable request from the authors.

Appendix A. Repumping

Because some of the observed transitions decay rather slowly and do not completely disappear in one temporal window, we take into account re-pumping of the slow TRPL component τ_1 from previous pulses, which leads to a 'background' increase as can be seen in figure A1, complicating a proper extraction of the background signal for individual wavelengths and correct time-constant extraction. This issue is overcome in TDPL by disentangling individual transitions by line-shape model fitting, where the slowest decay is assigned to (mainly non-radiative) pair recombination processes of DAPs in GaP [46, 47].

ORCID iDs

Petr Steindl https://orcid.org/0000-0001-9059-9202
Elisa Maddalena Sala https://orcid.org/0000-0001-8116-8830
Benito Alén https://orcid.org/0000-0003-3939-1611
Dieter Bimberg https://orcid.org/0000-0003-0364-6897
Petr Klenovský https://orcid.org/0000-0003-1914-164X

References

[1] Bimberg D, Kirstaedter N, Ledentsov N N, Alferov Z I, Kop'ev P S and Ustinov V M 1997 InGaAs-GaAs quantum-dot lasers *IEEE J. Sel. Top. Quantum Electron.* **3** 196–205
[2] Ledentsov N N *et al* 2003 *Electron. Lett.* **39** 1126
[3] Heinrichsdorff F, Mao M-H, Kirstaedter N, Krost A, Bimberg D, Kosogov A O and Werner P 1997 Room-temperature continuous-wave lasing from stacked InAs/GaAs quantum dots grown by metalorganic chemical vapor deposition *Appl. Phys. Lett.* **71** 22–4
[4] Bimberg D 2008 Quantum dot based nanophotonics and nanoelectronics *Electron. Lett.* **44** 168–71
[5] Azuma K, Tamaki K and Lo H-K 2015 All-photonic quantum repeaters *Nat. Commun.* **6** 6787
[6] Li Z-D *et al* 2019 Experimental quantum repeater without quantum memory *Nat. Photon.* **13** 644–8
[7] Lochmann A, Stock E, Schulz O, Hopfer F, Bimberg D, Haisler V A, Toropov A I, Bakarov A K and Kalagin A K 2006 Electrically driven single quantum dot polarised single photon emitter *Electron. Lett.* **42** 40–1
[8] Müller T *et al* 2018 A quantum light-emitting diode for the standard telecom window around 1550 nm *Nat. Commun.* **9** 862
[9] Martín-Sánchez J *et al* 2009 Single photon emission from site-controlled InAs quantum dots grown on GaAs(001) patterned substrates *ACS Nano* **3** 1513–7
[10] Schlehahn A *et al* 2015 Single-photon emission at a rate of 143 MHz from a deterministic quantum-dot microlens triggered by a mode-locked vertical-external-cavity surface-emitting laser *Appl. Phys. Lett.* **107** 041105
[11] Paul M, Olbrich F, Höschele J, Schreier S, Kettler J, Portalupi S L, Jetter M and Michler P 2017 Single-photon emission at 1.55 μm from MOVPE-grown InAs quantum dots on InGaAs/GaAs metamorphic buffers *Appl. Phys. Lett.* **111** 033102
[12] Salter C L, Stevenson R M, Farrer I, Nicoll C A, Ritchie D A and Shields A J 2010 An entangled-light-emitting diode *Nature* **465** 594–7
[13] Aberl J, Klenovský P, Wildmann J S, Martín-Sánchez J, Fromherz T, Zallo E, Humlíček J, Rastelli A and Trotta R 2017 Inversion of the exciton built-in dipole moment in In(Ga)As quantum dots via nonlinear piezoelectric effect *Phys. Rev.* B **96** 045414
[14] Klenovský P, Steindl P, Aberl J, Zallo E, Trotta R, Rastelli A and Fromherz T 2018 Effect of second-order piezoelectricity on the excitonic structure of stress-tuned In(Ga)As/GaAs quantum dots *Phys. Rev.* B **97** 245314
[15] Senellart P, Solomon G and White A 2017 High-performance semiconductor quantum-dot single-photon sources *Nat. Nanotechnol.* **12** 1026
[16] Csontosová D and Klenovský P 2020 Theory of magneto-optical properties of neutral and charged excitons in GaAs/AlGaAs quantum dots *Phys. Rev.* B **102** 125412
[17] Lim Y L, Beige A and Kwek L C 2005 Repeat-until-success linear optics distributed quantum computing *Phys. Rev. Lett.* **95** 030505
[18] Lindner N H and Rudolph T 2009 Proposal for pulsed on-demand sources of photonic cluster state strings *Phys. Rev. Lett.* **103** 113602
[19] Istrati D *et al* 2020 Sequential generation of linear cluster states from a single photon emitter *Nat. Commun.* **11** 5501
[20] Steindl P *et al* 2021 Artificial coherent states of light by multiphoton interference in a single-photon stream *Phys. Rev. Lett.* **126** 143601
[21] Marent A, Nowozin T, Geller M and Bimberg D 2011 The QD-flash: a quantum dot-based memory device *Semicond. Sci. Technol.* **26** 014026
[22] Marent A and Bimberg D 2012 *US Patent* 9.424925
[23] Marent A, Geller M and Bimberg D 2009 A novel nonvolatile memory based on self-organized quantum dots *Microelectron. J.* **40** 492–5
[24] Bimberg D, Marent A, Nowozin T and Schliwa A 2011 Antimony-based quantum dot memories *Quantum Dots and Nanostructures: Synthesis, Characterization, and Modeling VIII* (San Francisco, California, United States, 1 March 2011) vol 7947
[25] Marent A, Geller M, Schliwa A, Feise D, Pötschke K, Bimberg D, Akçay N and Öncan N 2007 106 years extrapolated hole storage time in GaSb/AlAs quantum dots *Appl. Phys. Lett.* **91** 242109
[26] Sala E M 2018 Growth and characterization of antimony-based quantum dots in GaP matrix for nanomemories *Doctoral Thesis* Technische Universität Berlin, Berlin
[27] Sala E M, Arikan I F, Bonato L, Bertram F, Veit P, Christen J, Strittmatter A and Bimberg D 2018 MOVPE-growth of InGaSb/AlP/GaP(001) quantum dots for nanoscale memory applications *Phys. Status Solidi* B **255** 1800182
[28] Klenovský P, Schliwa A and Bimberg D 2019 Electronic states of (InGa)(AsSb)/GaAs/GaP quantum dots *Phys. Rev.* B **100** 115424
[29] Burkard G, Loss D and DiVincenzo D P 1999 Coupled quantum dots as quantum gates *Phys. Rev.* B **59** 2070–8
[30] Křápek V, Klenovský P, Rastelli A, Schmidt O G and Munzar D 2010 Quantum entanglement in lateral GaAs/AlGaAs quantum dot molecules *J. Phys.: Conf. Ser.* **245** 012027
[31] Klenovský P, Křápek V and Humlíček J 2016 Type-II InAs/GaAsSb/GaAs quantum dots as artificial quantum dot molecules *Acta Phys. Pol.* A **129** A62–5
[32] Kapteyn C M A, Heinrichsdorff F, Stier O, Heitz R, Grundmann M, Zakharov N D, Bimberg D and Werner P 1999 Electron escape from InAs quantum dots *Phys. Rev.* B **60** 14265–8
[33] Bonato L, Sala E M, Stracke G, Nowozin T, Strittmatter A, Ajour M N, Daqrouq K and Bimberg D 2015 230 s room-temperature storage time and 1.14 eV hole localization energy in $In_{0.5}Ga_{0.5}As$ quantum dots on a GaAs interlayer in GaP with an AlP barrier *Appl. Phys. Lett.* **106** 042102

[34] Stracke G, Sala E M, Selve S, Niermann T, Schliwa A, Strittmatter A and Bimberg D 2014 Indirect and direct optical transitions in In0.5Ga0.5As/GaP quantum dots *Appl. Phys. Lett.* **104** 123107

[35] Nowozin T, Bimberg D, Daqrouq K, Ajour M N and Awedh M 2013 Materials for future quantum dot-based memories *J. Nanomater.* **1–6** 215613

[36] Steindl P, Sala E M, Alén B, Marrón D F, Bimberg D and Klenovský P 2019 Optical response of (InGa)(AsSb)/GaAs quantum dots embedded in a gap matrix *Phys. Rev.* B **100** 195407

[37] Grassman T J, Carlin J A, Galiana B, Yang L-M, Yang F, Mills M J and Ringel S A 2013 Nucleation-related defect-free GaP/Si(100) heteroepitaxy via metal-organic chemical vapor deposition *Appl. Phys. Lett.* **102** 142102

[38] Sala E M *et al* 2016 Growth and structure of In0.5Ga0.5Sb quantum dots on GaP(001) *Appl. Phys. Lett.* **109** 102102

[39] Gajjela R S R *et al* 2021 Structural and compositional analysis of (InGa)(AsSb)/GaAs/GaP Stranski–Krastanov quantum dots *Light Sci. Appl.* **10** 125

[40] Birner S, Zibold T, Andlauer T, Kubis T, Sabathil M, Trellakis A and Vogl P 2007 *IEEE Trans. Electron Devices* **54** 2137

[41] Zibold T 2007 *PhD Thesis* Technische Universität München

[42] Abramkin D S, Gutakovskii A K and Shamirzaev T S 2018 Heterostructures with diffused interfaces: luminescent technique for ascertainment of band alignment type *J. Appl. Phys.* **123** 115701

[43] Prieto J A, Armelles G, Pistol M-E, Castrillo P, Silveira J P and Briones F 1997 Optical studies of GaAs quantum wells strained to GaP *Appl. Phys. Lett.* **70** 3449–51

[44] Almosni S *et al* 2016 Correlations between electrical and optical properties in lattice-matched GaAsPN/GaP solar cells *Sol. Energy Mater. Sol. Cells* **147** 53–60

[45] Amtout A 1995 Calculation of the line shape of one-phonon replicas in polar semiconductors having direct forbidden band gaps *Phys. Rev.* B **52** 13955–64

[46] Dean P J, Henry C H and Frosch C J 1968 Infrared donor–acceptor pair spectra involving the deep oxygen donor in gallium phosphide *Phys. Rev.* **168** 812–6

[47] Dean P J 1970 Recombination processes associated with 'deep states' in gallium phosphide *J. Lumin.* **1–2** 398–419

[48] Klenovský P, Steindl P and Geffroy D 2017 Excitonic structure and pumping power dependent emission blue-shift of type-II quantum dots *Sci. Rep.* **7** 45568

[49] Jo M, Sato M, Miyamura S, Sasakura H, Kumano H and Suemune I 2012 Origin of the blueshift of photoluminescence in a type-II heterostructure *Nanoscale Res. Lett.* **7** 654

[50] Ledentsov N N *et al* 1995 Radiative states in type-II GaSb/GaAs quantum wells *Phys. Rev.* B **52** 14058–66

[51] Jin C Y, Liu H Y, Zhang S Y, Jiang Q, Liew S L, Hopkinson M, Badcock T J, Nabavi E and Mowbray D J 2007 Optical transitions in type-II InAs/GaAs quantum dots covered by a GaAsSb strain-reducing layer *Appl. Phys. Lett.* **91** 021102

[52] Gradkowski K, Ochalski T J, Williams D P, Healy S B, Tatebayashi J, Balakrishnan G, O'Reilly E P, Huyet G and Huffaker D L 2009 Coulomb effects in type-II Ga(As)Sb quantum dots *Phys. Status Solidi* B **246** 752–5

[53] Supplemental information (URL to be inserted by publisher).

[54] Gourdon C and Lavallard P 1989 Exciton transfer between localized states in $CdS_{1-x}Se_x$ alloys *Phys. Status Solidi* B **153** 641–52

[55] Rubel O, Stolz W and Baranovskii S D 2007 Spectral dependence of the photoluminescence decay in disordered semiconductors *Appl. Phys. Lett.* **91** 021903

[56] Sugisaki M, Ren H-W, Nishi K, Sugou S and Masumoto Y 2000 Excitons at a single localized center induced by a natural composition modulation in bulk $Ga_{0.5}In_{0.5}P$ *Phys. Rev.* B **61** 16040–4

[57] Su Z and Xu S 2017 A generalized model for time-resolved luminescence of localized carriers and applications: dispersive thermodynamics of localized carriers *Sci. Rep.* **7** 13

[58] Oueslati M, Benoit C and Zouaghi M 1988 Resonant Raman scattering on localized states due to disorder in $GaAs_{1-x}P_x$ alloys *Phys. Rev.* B **37** 3037–41

[59] Johansen J, Stobbe S, Nikolaev I S, Lund-Hansen T, Kristensen P T, Hvam J, Vos W L and Lodahl P 2008 Size dependence of the wavefunction of self-assembled InAs quantum dots from time-resolved optical measurements *Phys. Rev.* B **77** 1–4

[60] Johansen J, Julsgaard B, Stobbe S, Hvam J M and Lodahl P 2010 Probing long-lived dark excitons in self-assembled quantum dots *Phys. Rev.* B **81** 1–4

[61] Shamirzaev T S, Abramkin D S, Gutakovskii A K and Putyato M A 2010 High quality relaxed GaAs quantum dots in gap matrix *Appl. Phys. Lett.* **97** 023108

[62] Zollner S, Gopalan S and Cardona M 1989 Intervalley deformation potentials and scattering rates in zinc blende semiconductors *Appl. Phys. Lett.* **54** 614–6

[63] Sosnowski T S, Norris T B, Jiang H, Singh J, Kamath K and Bhattacharya P 1998 Rapid carrier relaxation in $In_{0.4}Ga_{0.6}As$/GaAs quantum dots characterized by differential transmission spectroscopy *Phys. Rev.* B **57** R9423–6

[64] Robert C *et al* 2012 Electronic, optical, and structural properties of (In, Ga)As/GaP quantum dots *Phys. Rev.* B **86** 205316

[65] Robert C *et al* 2016 Electronic wave functions and optical transitions in (In, Ga)As/GaP quantum dots *Phys. Rev.* B **94** 075445

[66] Abramkin D S, Putyato M A, Budennyy S A, Gutakovskii A K, Semyagin B R, Preobrazhenskii V V, Kolomys O F, Strelchuk V V and Shamirzaev T S 2012 Atomic structure and energy spectrum of Ga(As, P)/GaP heterostructures *J. Appl. Phys.* **112** 083713

[67] Abramkin D S, Putyato M A, Gutakovskii A K, Semyagin B R, Preobrazhenskii V V and Shamirzaev T S 2012 New system of self-assembled GaSb/GaP quantum dots *Semiconductors* **46** 1534–8

[68] Mannik L, Jedral L and Ruda H E 1992 Decay of green photoluminescence in GaP: Zn, O *Phys. Rev.* B **46** 3826–9

[69] Moser K, Baumgartner R and Prettl W 1984 Decay of the red Cu-S pair luminescence in GaP *Solid State Commun.* **49** 761–4

[70] Llorens J M *et al* 2019 Topology driven *g*-factor tuning in type-II quantum dots *Phys. Rev. Appl.* **11** 044011

[71] Rautert J, Shamirzaev T S, Nekrasov S V, Yakovlev D R, Klenovský P, Kusrayev Yu G and Bayer M 2019 Optical orientation and alignment of excitons in direct and indirect band gap (In, Al)As/AlAs quantum dots with type-I band alignment *Phys. Rev.* B **99** 195411

[72] Schimpf C *et al* 2019 Resolving the temporal evolution of line broadening in single quantum emitters *Opt. Express* **27** 35290–307

[73] Manna U, Zhang Q, Dhomkar S, Salakhutdinov I F, Tamargo M C, Noyan I C, Neumark G F and Kuskovsky I L 2012 Radiative transitions in stacked type-II ZnMgTe quantum dots embedded in ZnSe *J. Appl. Phys.* **112** 063521

[74] Alonso-Álvarez D 2011 Strain balanced epitaxial stacks of quantum dots and posts *PhD Thesis, Dissertation* Universidad Autónoma de Madrid

[75] Gurioli M, Vinattieri A, Colocci M, Deparis C, Massies J, Neu G, Bosacchi A and Franchi S 1991 *Phys. Rev.* B **44** 3115–24

[76] Daly E M, Glynn T J, Lambkin J D, Considine L and Walsh S 1995 Behavior of $In_{0.48}Ga_{0.52}P$ quantum-well luminescence as a function of temperature *Phys. Rev.* B **52** 4696–9

[77] Oberli D Y, Dupertuis M-A, Reinhardt F and Kapon E 1999 Effect of disorder on the temperature dependence of radiative lifetimes in V-groove quantum wires *Phys. Rev.* B **59** 2910
[78] Citrin D S 1993 Radiative lifetimes of excitons in quantum wells: localization and phase-coherence effects *Phys. Rev.* B **47** 3832–41
[79] Klenovský P, Křápek V, Munzar D and Humlíček J 2010 Modelling of electronic states in InAs/GaAs quantum dots with GaAsSb strain reducing overlayer *J. Phys.: Conf. Ser.* **245** 012086
[80] Klenovský P, Křápek V, Munzar D and Humlíček J 2010 Electronic structure of InAs quantum dots with GaAsSb strain reducing layer: localization of holes and its effect on the optical properties *Appl. Phys. Lett.* **97** 203107
[81] Klenovský P, Hemzal D, Steindl P, Zíková M, Křápek V and Humlíček J 2015 Polarization anisotropy of the emission from type-II quantum dots *Phys. Rev.* B **92** 241302(R)
[82] Dadgostar S 2016 (Al, Ga)(As, P) structures in the GaP matrix: growth and characterization *Doctoral Thesis* Humboldt-Universität Berlin, Berlin
[83] Skazochkin A V, Krutogolov Yu K and Kunakin Yu I 1995 Nature of some electron traps in GaP *Semicond. Sci. Technol.* **10** 634
[84] Ioffe Institute NSM archive—physical properties of semiconductors www.ioffe.rssi.ru (accessed 7 October 2021)
[85] Abramkin D S, Petrushkov M O, Putyato M A, Semyagin B R, Emelyanov E A, Preobrazhenskii V V, Gutakovskii A K and Shamirzaev T S 2019 GaAs/GaP quantum-well heterostructures grown on Si substrates *Semiconductors* **53** 1143–7
[86] Desplanque L, Coinon C, Troadec D, Ruterana P, Patriarche G, Bonato L, Bimberg D and Wallart X 2017 Morphology and valence band offset of GaSb quantum dots grown on GaP(001) and their evolution upon capping *Nanotechnology* **28** 225601
[87] Nowozin T 2014 Self-Organized quantum dots for memories, electronic properties and carrier dynamics *Doctoral Thesis* Technische Universität Berlin, Berlin
[88] Sala E M, Godsland M, Trapalis A and Heffernan J 2021 Effect of cap thickness on InAs/InP quantum dots grown by droplet epitaxy in metal-organic vapor phase epitaxy *Phys. Status Solidi RRL* **15** 2100283
[89] Emberger V, Hatami F, Ted Masselink W and Peters S 2013 AlP/GaP distributed Bragg reflectors *Appl. Phys. Lett.* **103** 1–5
[90] Rauter P, Spindlberger L, Schäffler F, Fromherz T, Freund J and Brehm M 2018 Room-temperature group-IV led based on defect-enhanced ge quantum dots *ACS Photonics* **5** 431–8
[91] Murphy-Armando F, Brehm M, Steindl P, Lusk M T, Fromherz T, Schwarz K and Blaha P 2021 Light emission from direct band gap germanium containing split-interstitial defects *Phys. Rev.* B **103** 85310